

Study of the $^{34}\text{Ar}(\alpha, p)^{37}\text{K}$ reaction rate via proton scattering on ^{37}K , and its impact on properties of modeled X-Ray bursts

A. Lauer-Coles,^{1,*} C. M. Deibel,¹ J. C. Blackmon,¹ A. Hood,¹ E. C. Good,¹ K. T. Macon,¹
D. Santiago-Gonzalez,² H. Schatz,³ T. Ahn,³ J. Browne,³ F. Montes,³ K. Schmidt,^{3,4} W. J.
Ong,^{3,†} K. A. Chippis,^{5,6} S. D. Pain,^{5,6} I. Wiedenhöver,⁷ L. T. Baby,⁷ N. Rijal,⁷ M. Anastasiou,⁷
S. Upadhyayula,^{8,9,‡} S. Bedoor,⁹ J. Hooker,^{8,9} E. Koshchiy,⁹ and G. V. Rogachev^{8,9}

¹*Louisiana State University Dept. of Physics & Astronomy, Baton Rouge, LA, 70802*

²*Argonne National Laboratory, Lemont, IL, 60439*

³*Department of Physics and Astronomy and National Superconducting Cyclotron Laboratory,
Michigan State University, East Lansing, Michigan 48824*

⁴*Institute of Radiation Physics, Helmholtz-Zentrum Dresden-Rossendorf,
Bautzner Landstr. 400, 01328 Dresden, Germany*

⁵*Physics Division, Oak Ridge National Laboratory, Oak Ridge, Tennessee 37831*

⁶*Department of Physics and Astronomy, University of Tennessee, Knoxville, Tennessee 37996*

⁷*Physics Department, Florida State University, Tallahassee, Florida, 32306*

⁸*Department of Physics and Astronomy, Texas A&M University, College Station, Texas 77843, USA*

⁹*Cyclotron Institute, Texas A&M University, College Station, Texas 77483*

(Dated: November 18, 2024)

Background: Type I X-Ray bursts (XRBs) are energetic stellar explosions that occur on the surface of a neutron star in an accreting binary system with a low-mass H/He-rich companion. The rate of the $^{34}\text{Ar}(\alpha, p)^{37}\text{K}$ reaction may influence features of the light curve that results from the underlying thermonuclear runaway, as shown in recent XRB stellar modelling studies.

Purpose: In order to reduce the uncertainty of the rate of this reaction, properties of resonances in the compound nucleus ^{38}Ca , such as resonance energies, spins, and particle widths, must be well constrained.

Method: This work discusses a study of resonances in the ^{38}Ca compound nucleus produced in the $^{34}\text{Ar}(\alpha, p)$ reaction. The experiment was performed at the National Superconducting Cyclotron Laboratory, with the ReA3 facility by measuring proton scattering using an unstable ^{37}K beam. The kinematics were designed specifically to identify and characterize resonances in the Gamow energy window for the temperature regime relevant to XRBs.

Results: The spins and proton widths of newly identified and previously known states in ^{38}Ca in the energy region of interest for the $^{34}\text{Ar}(\alpha, p)^{37}\text{K}$ reaction have been constrained through an R-Matrix analysis of the scattering data.

Conclusions: Using these constraints, a newly estimated rate is applied to an XRB model built using Modules for Experiments in Stellar Astrophysics (MESA), to examine its impact on observables, including the light curve. It is found that the newly determined reaction rate does not substantially affect the features of the light curve.

arXiv:2411.09918v1 [nucl-ex] 15 Nov 2024

* Present address: Savannah River National Laboratory, Savannah River Site, SC, 29803; acoles@bnl.gov; www.amberlauercoles.com

† Present address: Nuclear and Chemical Sciences Division, Lawrence Livermore National Laboratory, Livermore CA, USA 94550

‡ Present address: Lawrence Livermore National Laboratory, 7000 East Ave, Livermore, CA 94550, USA

I. INTRODUCTION

Type I X-Ray Burst (XRB) nucleosynthesis occurs when H- and He-rich material is accreted onto the surface of a neutron star. This happens when the neutron star is in a low-mass ($< 1 - 2 M_{\odot}$) X-ray binary system with a hydrogen- and/or helium-rich donor, such as a main sequence star. The surface material then seeds the resulting nuclear reactions, which first consist of nuclear burning that occurs on the surface during accretion through the Hot Carbon-Nitrogen-Oxygen (HCNO) cycles, and then the thermonuclear runaway during the XRB. This runaway occurs when surface thermodynamic conditions reach extreme levels related to a critical accretion rate, leading to a thin-shell instability [1]. In this mildly degenerate shell, thermal energy from nucleosynthesis is not dissipated, and instead feeds back into the rising thermodynamics, resulting in a shell-flash. The triple-alpha (3α) process drives this flash, and the energy released allows alternate reactions to bypass the time-limited steps in the HCNO cycle until finally a breakout reaction routes into the runaway thermonuclear nucleosynthesis known as the XRB. The burst is identified by the primary observable, a release of photons in the X-ray spectrum, known as the “light-curve” characterized by a rapid increase in flux, followed by an exponential decay. Type I XRB’s can last $10 - 100$ s, reach peak temperatures of $1 - 2$ GK, recur over periods of hours to days, and release $10^{39} - 10^{40}$ ergs of energy.

The thermonuclear runaway is fueled during the rise time by the (α, p) process, a series of (α, p) and (p, γ) reactions. During the exponential decay of the burst the rp (rapid proton-capture) process occurs, via a series of (p, γ) reactions and β decays ending around $A = 100$ [2]. Several of the (α, p) reactions in the former process occur on so-called waiting-point nuclei. In these even-even, $(Z - N)/2 = 1$ nuclei the radiative proton captures and the corresponding photo-disintegration are in a $(p, \gamma) - (\gamma, p)$ equilibrium, due to their low $Q_{p, \gamma}$ -values. Without an alternate pathway, nucleosynthesis may stall due to the β^+ -decay half-life (~ 1 s), which is comparable to the timescale of the burst. An (α, p) reaction, once the temperature is sufficiently high, offers an alternative route for the nucleosynthesis, thus restarting the burst. Such a stalling and restarting of the nucleosynthesis may be responsible for observed double-peaked XRBs (e.g. [3]). There are four common candidates for waiting point nuclei in the (α, p) process, ^{22}Mg , ^{26}Si , ^{30}S , and ^{34}Ar [4], and an additional possible candidate, ^{38}Ca , identified in [5]. In standard, single-peaked bursts, the waiting point nuclei would still be expected to impact burst features.

Several published stellar models indeed indicate that the $^{34}\text{Ar}(\alpha, p)^{37}\text{K}$ rate influences observables and other relevant quantities [4, 6, 7]. Specifically, Fisker *et al.* [4] showed that $^{34}\text{Ar}(\alpha, p)^{37}\text{K}$ may affect the magnitude of the dip in a double-peaked burst. Cyburt *et al.* [6] in a 2016 XRB sensitivity study showed that this reaction may also influence the burst luminosity. Finally, in Parikh *et al.* [7], variation in the rate was found to affect the ^{34}S abundance.

Due to low cross sections of the reaction and the low intensities of available ^{34}Ar beams, the $^{34}\text{Ar}(\alpha, p)^{37}\text{K}$ reaction has only been studied directly once by Browne *et al.* [8], though at energies well above the astrophysically relevant energy regime. It has yet to be incorporated into rate formulations in the standard REACLIB library. As such, the theoretical rate calculation found in REACLIB [9] is the standard value used in many stellar models. However, the underlying Hauser-Feshbach formalism used in cases where experimental values are not available, may be inappropriate if the reaction rate is dominated by a small number of resonances in the ^{38}Ca compound nucleus [10].

A previous indirect measurement at iThemba Laboratories studied the $^{40}\text{Ca}(p, t)^{38}\text{Ca}$ reaction using the K= 600 spectrograph [11]. This measurement confirmed 14 previously observed levels and detected more than 30 new levels between the ground state and $E_x = 13$ MeV, with ~ 20 of these within the Gamow widow for $T_9 = 1.5$ GK. This result agrees with measurements of the mirror nucleus, ^{38}Ar , which contains approximately the same number of s -wave resonances within this region [12]. These results were used to calculate a new $^{34}\text{Ar}(\alpha, p)^{37}\text{K}$ reaction rate, which is lower by up to two orders of magnitude in the Gamow window when compared with TALYS V1.8 and NON-SMOKER^{web}/REACLIB calculations. This discrepancy is however not seen in the recent study by Browne *et al.* [8], which used a Si detector array with the Jet Experiments in Nuclear Structure and Astrophysics (JENSA) gas jet target [13] for a direct measurement using an ^{34}Ar beam from ReA3. Two measurements were taken at $E_{cm} = 5.6$ and 5.9 MeV and the resulting cross sections are consistent with the Hauser-Feshbach-calculated value of this rate. However, that study was not able to disentangle contributions from (α, p) reactions on the beam contaminants and the data obtained was above the astrophysically relevant energy regime of $E_{cm} = 2.0 - 3.9$ MeV.

Here we report on a measurement of proton scattering on ^{37}K (Sec. II) to study properties of states in the compound nucleus, ^{38}Ca , important for estimating the $^{34}\text{Ar}(\alpha, p)^{37}\text{K}$ reaction rate. The excitation spectrum resulting from this experiment and previously known resonance energies were analyzed in an R -matrix calculation to constrain spin-parity values and partial widths of these resonances and to identify additional resonances previously unobserved (Sec. III). These quantities, together with theoretical α and proton widths, were used to calculate the reaction rate via the narrow-resonance formalism (Sec. IV), which is compared to other existing rate calculations. It was then input into models of an XRB in the stellar evolution software MESA. The results of these models are then compared with a baseline model and previous models in Sec. V.

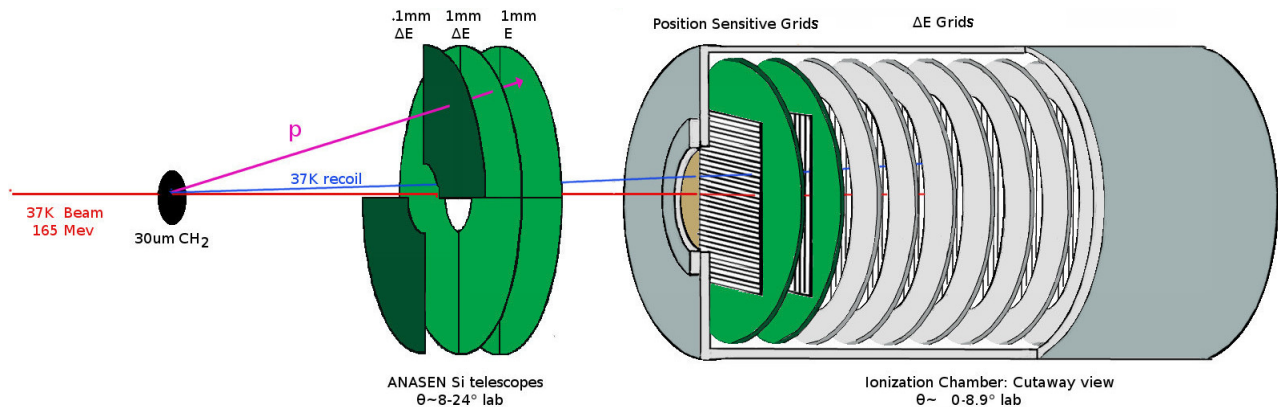


FIG. 1. A mock-up of the experimental setup. The ^{37}K beam impinges on the polypropylene target, with the lighter product, the protons, emitted at larger angles and entering the silicon telescope. The heavier products and the unreacted beam are forward focused into the ionization chamber (IC). The green wire grids in the IC are printed circuit boards that provide position sensitivity, while signals from the gray grids are combined in sequence in adjustable groups to measure energy loss and total energy of the particles.

II. EXPERIMENTAL DESIGN

The experiment was performed at the ReA3 facility at the National Superconducting Cyclotron Laboratory (NSCL) at Michigan State University using a radioactive ion beam of ^{37}K ($t_{1/2} = 1.23$ s). A primary beam of ^{40}Ca from the K500 & K1200 coupled cyclotrons bombarded a ^9Be production target. The A1900 magnetic fragment separator was used to select ^{37}K from the resulting isotopes. A gas catcher then collected these ions and fed them into the Electron Beam Ion Trap charge breeder to produce $^{37}\text{K}^{2+}$ ions. These were injected into the ReA3 linear accelerator to produce a final beam of 4.448 MeV/u with $\sim 87\%$ purity and an intensity of $\sim 10^4$ pps delivered to the experimental area.

The beam impinged on a 2.7-mg/cm^2 CH_2 target to produce the desired proton-scattering events. Protons emitted at $\theta_{lab} = 15.4 - 28.2^\circ$ were detected by Si detector telescopes arranged in quadrants as shown in Fig. 1. Two opposite quadrants consisted of a stack of two 1-mm thick Si detectors (both Micron Semiconductor model QQQ3). The other two quadrants comprised a stack of three Si detectors (Micron Semiconductor models QQQ5) with a 0.1-mm thick ΔE detector backed by two additional Si detectors of 1-mm thickness each. However, the thresholds in the ASIC electronics for detection of the low energies deposited by the protons in the 0.1-mm-thick detectors was found to be unreliable. Thus, in the subsequent analysis, data is only presented from the QQQ3 detectors. A self-consistent energy calibration was performed by combining the dominant ^{241}Am characteristic α decays ($E_\alpha = 5.486$ MeV) and signals from an electronic pulser. The heavy ions (beam, contaminants, and heavy recoil products) were forward focused and passed through the center of the silicon telescopes to enter the Ionization Chamber (IC) [14], which provided both position and Z identification by relative energy loss. The different elemental components of the beam were clearly resolved in the ionization chamber when a target was not in place, allowing the beam composition to be periodically monitored and optimized. Contaminants in the beam ($\sim 13\%$ of the beam) were nearly equal parts ^{37}Cl and ^{37}Ar . With the CH_2 target in place, the Z resolution of the IC was not sufficient to discriminate scattering from the elemental components on an event-by-event basis.

Protons arising from scattering were selected by a gate on the timing coincidence between the IC and the Si telescopes. Background protons produced through $^{37}\text{K} + ^{12}\text{C}$ fusion evaporation were highly suppressed as the majority of heavy recoils from this process are stopped in the IC window or dead space (i.e. the small IC volume upstream of the wire grids) due to their high Z and low energy. Additionally, a 3.2-mg/cm^2 carbon target was inserted to measure the contributions from $^{37}\text{K} + ^{12}\text{C}$ fusion evaporation, which produced only a small featureless background when the relevant Si-IC timing gate was applied. This background extended to energies higher than the scattered protons, allowing the level of fusion evaporation contamination to also be quantified in the scattering data where it was determined to comprise less than 5% of the observed events.

III. ANALYSIS

The segmented QQQ3 silicon detectors (16 rings and 16 sectors) measured the reaction angle for each event. Kinematic reconstruction converted the measured proton energy and angle of the elastic scattering events from the

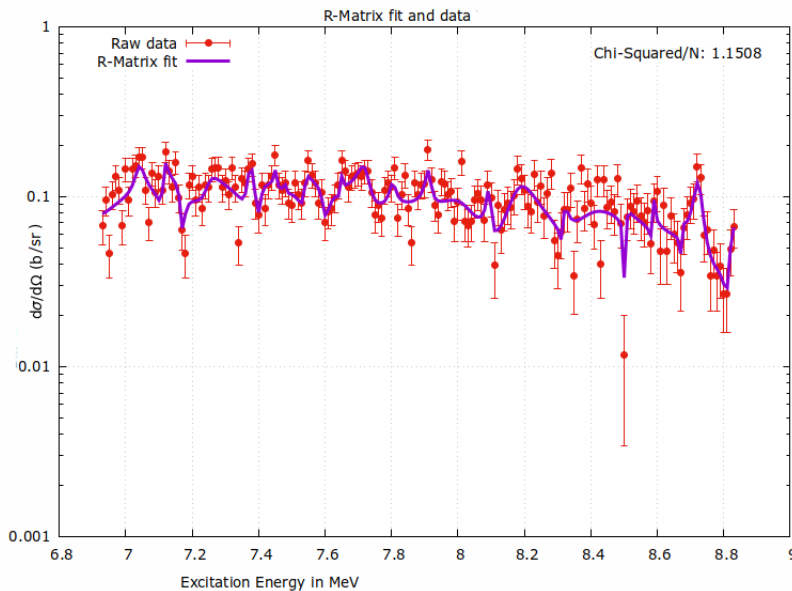


FIG. 2. Differential cross section of proton-scattering on ^{37}K measured in this work. The data is presented in forward-kinematic lab frame, the required frame for AZURE2 calculations. Also pictured is a characteristic R-matrix fit from the process described in Sec. III and the corresponding goodness-of-fit statistic, χ^2/N .

lab frame into center-of-mass, combining data over the entire detector into a single excitation function corresponding to an average detector lab angle of 22.2° (center-of-mass angle of 135.7°). An absolute energy calibration was applied to the excitation function using proton-scattering data taken with an ^{40}Ar stable beam and the same CH_2 target. This proton-scattering spectrum is well characterized by a previous study [15] with two distinctive resonant features that were aligned with the same features in the ^{40}Ar stable beam spectrum to provide a two-point calibration. The final, calibrated spectrum from proton scattering on ^{37}K , converted to excitation energy in ^{38}Ca in the range of $E_x = 6.92 - 8.82$ MeV, is shown in Fig. 2.

The excitation function was analyzed using the *R*-matrix formalism [16] performed with AZURE2 [17]. A channel radius of $a = 6.065$ fm was used, estimated from $R = R_0(A_1^{1/3} + A_2^{1/3})$ with a suitably large $R_0 \sim 1.4$ fm to be outside of the range of the nuclear force for the $A = 38$ compound nucleus. Previously observed states within the energy range shown in Fig. 2 were included with their energy values held fixed to the those reported in [11]. A good fit to the excitation function could not be obtained using only these levels.

Only natural-parity states contribute to the $^{34}\text{Ar}(\alpha, p)^{37}\text{K}$ reaction due to the 0^+ total channel spin for the $^{34}\text{Ar} + \alpha$ system. While population of natural-parity states is favored in the $^{40}\text{Ca}(p, t)^{38}\text{Ca}$ reaction [11], unnatural parity states can be strongly populated in $^{37}\text{K} + p$ scattering, so the need for additional states is expected. We added additional hypothetical levels to the *R*-matrix model with energies initially set to the most prominent features in the data. This resulted in a total of 24 states being included in the analysis (13 of which are newly identified here), which is consistent with the level density found in the mirror nucleus ^{38}Cl . With few experimental constraints on resonance properties, the resulting large size of the parameter space and likelihood for many local minima required implementing some assumptions in the analysis.

We included only proton partial widths corresponding to protons populating the ground state in ^{37}K . The lowest-energy part of the excitation function ($E_x < 7.9$ MeV) may have some contamination from proton inelastic scattering originating from the upstream half of the target that populates the first-excited state in ^{37}K at 1.37 MeV. However, the observed yield of protons with energies too low to correspond to elastic scattering indicates that this contribution is likely negligible.

Only the lowest orbital angular momentum value was included for any state's particular J^π , but both possible channel-spin combinations were included [18]. We initially fixed all the resonance energies. Initial values for partial widths were chosen that were comparable to the size of features in the excitation function or the experimental resolution from Ref. [11]. The excitation function was fit using MINUIT2 varying partial widths constrained to be within a limited range, varying by no more than a factor of 1.7. Once a local minimum was obtained within this restricted parameter space, the J^π value of a randomly selected state was changed, and the gradient fit repeated. The process of randomly changing a J^π value and repeating a gradient fit was iterated, starting each cycle with the best previous fit, until no improvement was gained.

TABLE I. Resonances with suggested spin-parity assignments and partial widths. Resonances not previously identified in [11] are indicated with *. The systematic uncertainty is indicated with a $^\circ$, while † indicates statistical uncertainties estimated by calculating the fraction of the reduced width amplitude (RWA) uncertainties to the actual RWA value and applying the same ratio to the partial width.

$E_x(\text{MeV})$	J^π	$\Gamma_p(\text{keV}) (\pm u^\circ) (u_+^\dagger)(u_-^\dagger)$	$E_x(\text{MeV})$	J^π	$\Gamma_p(\text{keV}) (\pm u^\circ) (u_+^\dagger)(u_-^\dagger)$
7.041(8)	2^+	33(5)(8)(14)	7.884(23)*	$1^+/3^+$	21(10)(4)(5)
7.108(11)*	$1^-/1^+$	26(12)(17)(8)	8.026(5)	$0^+/1^-/2^+$	6(4)(3)(1)
7.176(4)	3^-	25(3)(24)(23)	8.097(3)*	$1^+/2^-/3^-$	12(3)(6)(7)
7.243(8)*	1^+	76(33)(24)(19)	8.132(15)*	$1^+/3^-$	73(2)(70)(36)
7.37(5)	2^+	31(7)(8)(7)	8.189(6)	2^+	57(47)(145)(31)
7.411(11)*	$1^+/3^-$	36(7)(43)(72)	8.322(5)	2^+	9(12)(14)(5)
7.4504(6)*	1^+	5(6)(79)(89)	8.363(9)*	1^+	22(3)(11)(13)
7.539(8)*	1^+	36(22)(55)(43)	8.491(11)*	1^+	5(2)(2)(4)
7.611(8)*	$1^+/3^-$	38(20)(26)(72)	8.507(9)	1^-	20(7)(9)(15)
7.647(9)*	1^+	45(19)(61)(53)	8.586(3)	2^+	87(78)(14)(13)
7.726(5)*	3^+	34(11)(14)(25)	8.672(6)	1^-	8(6)(7)(8)
7.801(3)	2^+	28(6)(9)(10)	8.717(8)	2^+	47(7)(14)(14)

This entire fitting process was repeated six times, varying J^π values in different ways each time. An example of one of the fits is shown in Fig. 2. Finally, fits were performed using the mean values from the results of these six fits as a starting point but varying the energies of previously-unidentified resonances in addition to the partial widths. The resulting fit converged to values close the initial input mean values (well within uncertainties).

Table I gives the final values for E_x , Γ_p , and J^π . For seven of the 24 states, multiple J^π values were found to provide a comparable fit. The partial widths given are an average of the six solutions. Uncertainties in the partial widths are provided that include a systematic analysis of the values from the six different fits and a statistical uncertainty calculated using the reduced width amplitude values returned from MINUIT2.

IV. REACTION RATE

The reaction rate is calculated using the narrow resonance approximation from the definition provided in [19], with the total reaction rate expressed as a sum over individual resonances described by the Breit-Wigner formalism:

$$N_A < \sigma v > = 1.54 \times 10^{11} (\mu T_9)^{-3/2} \sum_i (\omega\gamma)_i \exp\left(-\frac{11.605 E_i}{T_9}\right) \quad (1)$$

where μ is the reduced mass in amu, T_9 is the temperature in GK, E_i is the resonance energy in MeV, and $(\omega\gamma)_i$ is defined as the resonance strength (in MeV):

$$(\omega\gamma)_i = \frac{(2J_i + 1)}{(2j_1 + 1)(2j_2 + 1)} \frac{\Gamma_\alpha \Gamma_p}{\Gamma_{tot}} \approx (2J_i + 1) \Gamma_\alpha. \quad (2)$$

Here, Γ_α and Γ_p are the partial widths of the entrance (α) and exit (p) channels, respectively; Γ_{tot} is the total width of the resonance ($\Gamma_{tot} = \Gamma_\alpha + \Gamma_p + \Gamma_\gamma$ in this case), and J_i , j_1 and j_2 are the spins of the resonance and the reactants (α and ^{34}Ar in this case with $j_1 = j_2 = 0$), respectively. While the R -matrix formalism would be more appropriate given the level density in this case, the narrow-resonance approach of [11] is followed to allow a more direct comparison of the rates and impact.

The α partial width is related to the single-particle width, Γ_α^{sp} , thusly: $\Gamma_\alpha = C^2 S_\alpha \Gamma_\alpha^{sp}$, where $C^2 S_\alpha$ is the spectroscopic factor. The same constant spectroscopic factor of 0.01 used in Ref. [11] is used here for the α partial widths for consistency. In addition to this constant factor, a distribution of α spectroscopic factors set to mimic the existence of α -cluster states was used in a separate analysis by [11]; however, this structure has not been observed and thus is not explored in this work. Proton partial widths from the R -matrix analysis discussed above and estimated gamma partial widths were used to verify that $\Gamma_p \gg \Gamma_\gamma + \Gamma_\alpha$, implying resonance strengths can be accurately estimated using $(\omega\gamma)_i \approx (2J_i + 1) \Gamma_\alpha$.

The total reaction rate calculated here includes the new resonance information as well as additional levels reported in Ref. [11, 20], as the latter includes levels outside the experimental region explored here that still contribute to the overall reaction rate. The reaction rate was calculated 10^7 times using a Monte-Carlo sampling of spin assignments for each resonance. The distribution of spins was taken from Long *et al.* (see Fig. 3 in [11]).

Statistical analysis provides the recommended median rate, along with the 1st and 3rd quartile. The uncertainties are dominated by the uncertain spin-parities and alpha-partial widths of the states of interest. The resulting rate is presented in Fig. 3 along with the rates from the previous work by [11, 20], as well as REACLIB [6]. There is good agreement between the astrophysical reaction rate calculated in this work and Long *et al.* [11], varying by an average factor of .915, while both vary from the REACLIB Hauser Feschbach-based rate by approximately a factor of 45. This, however, disagrees with the conclusions of Browne *et al.* [8], which state that the Hauser-Feschbach estimate is likely sufficient for this reaction.

V. IMPACT ON STELLAR MODELS

The ultimate impact of this new reaction rate was tested using a Type-I X-ray Burst model adapted from Paxton *et al.* [21], Modules for Experiments with Stellar Astrophysics (MESA), version 10108. MESA is a multi-zone, 1D radial stellar evolution code, with adaptive mesh in time and space that includes relevant physics such as opacities, hydrodynamics, mixing length theory, atmospheric boundary conditions, and equation of state. The nuclear network differential equations are coupled to those that model the physical aspects so that the energy generation provides feedback into the thermodynamics and vice versa, and includes mixing between zones. The model is designed to simulate conditions of a hydrogen-dominant burst on GS 1826-24, colloquially known as the “clocked burster” due to its extreme regularity [22], with an initial neutron-star mass and radius of $1.4 M_{\odot}$ and 11.2 km, respectively. This model assumes solar abundances for accretion (${}^1\text{H} = 0.7048$, ${}^4\text{He} = 0.2752$, and Z from [23]) at a rate of $\sim 3 \times 10^{-9} M_{\odot}/\text{yr}$. The nuclear network is similar to the classic 304-species XRB network identified by [24], favoring proton-rich isotopes up to ${}^{107}\text{Te}$, but with the neutron-degenerate core modelled as the heavy element ${}^{138}\text{Ba}$, which is technically included in the nuclear network but is far above the next-greatest Z isotope and so unreachable by any standard capture reaction. The result is that the core is essentially inert. Additional astrophysical details of the model can be found in Ref. [21].

Here we report the results of 11 variations of the base model to test a sample of the range of known burst conditions with different ${}^{34}\text{Ar}(\alpha, p){}^{37}\text{K}$ reaction rates. For five models there was no alteration save the ${}^{34}\text{Ar}(\alpha, p){}^{37}\text{K}$ reaction rate. This set included the standard REACLIB rate, REACLIB $\times 100$ and $\times 0.01$, the recommended rate from this work, and REACLIB $\times 0.022$ (i.e. approximately the average ratio of this work to REACLIB). These factors were chosen to compare with similar published stellar modelling studies. The standard REACLIB rate is from the 2010 compilation of theoretical Hauser-Feschbach rate calculations [9].

Three additional models increased the He accretion percentage to 47% to mimic a He-rich companion and provide conditions where an α -induced reaction might be especially impactful. Three more models tested a slowed accretion ($7.93 \times 10^{-10} M_{\odot}/\text{yr}$) compared to the “clocked burster” model. These six models all used the ${}^{34}\text{Ar}(\alpha, p){}^{37}\text{K}$ REACLIB rate as the baseline with the same variations by factors of $\times 100$ and $\times 0.01$.

Finally, an additional three models changed the metallicity of the accreted material to a relatively high value of 0.19, about ten times Solar metallicity. This was done for comparison to the astrophysical scenario used in Parikh *et al.* [7], where the high- Z starting composition model resulted in the largest impact from varying the ${}^{34}\text{Ar}(\alpha, p){}^{37}\text{K}$ rate, altering the resulting abundance of ${}^{34}\text{S}$. In these models the starting metallicity was of a similar value as Parikh *et al.*, albeit slightly lower in order to produce a model that was numerically stable. Indeed, this group of models only exhibited one burst, after which the model was quiescent for an extended time and then unable to find suitable solutions to the differential equations such that evolution did not proceed and thus the results are not discussed here. It should be noted that Fisker *et al.* treated this high- Z scenario in the initial abundance, rather than the accretion, a scenario which is outside the scope of this work. It should also be noted that the single burst produced in this model was the only output light curve that exhibited a double peak.

ch is why I made up my own.

The models investigated here were compared via the following metrics: burst period (absolute and differential), integrated luminosity (definition given below), and maximum luminosity (absolute and differential). A summary of the results of the stellar modelling is given in Table II. The number of bursts is also listed, and gives a general sense of the numerical stability of the model, with more bursts corresponding to higher stability. The full set of stable burst models as well as the folded, averaged burst light curves, which are used to calculate integrated luminosity metric, are reflected in Figs. 4, 5, and 6. Final abundances were also tracked for this study; however, there were no significant differences in the final abundances produced by the bursts with the variation of the ${}^{34}\text{Ar}(\alpha, p){}^{37}\text{K}$ reaction rate.

The three different sets of models result in differences in the burst duration from each other, but as this was not

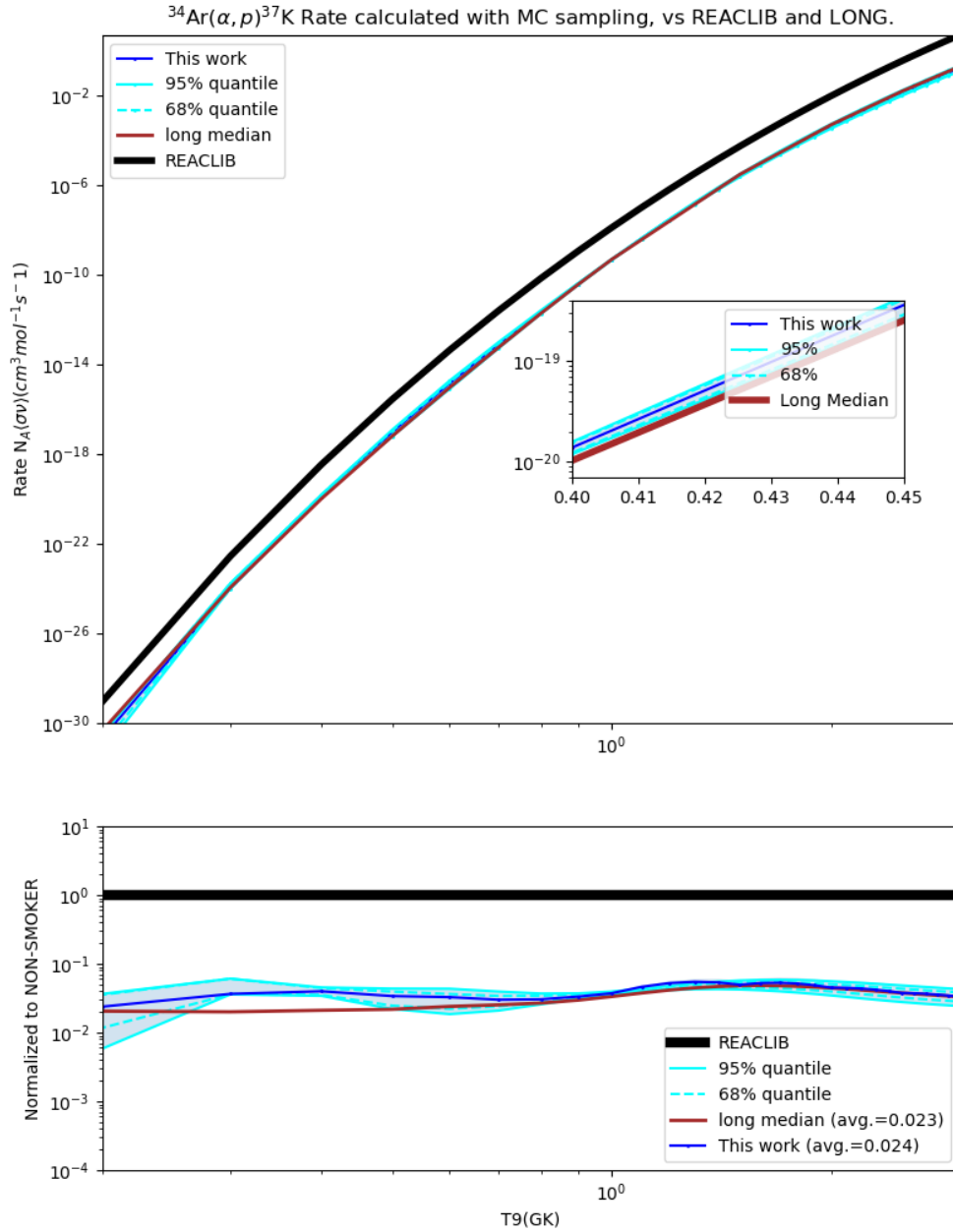


FIG. 3. (TOP) The final astrophysical reaction rate calculated from Monte Carlo sampling is depicted here along with the 68% and 95% quantiles. The REACLIB rate is also shown, as well as the rate calculated in Long *et al.*[11]. (BOTTOM) The ratio of the rates depicted above normalized to REACLIB.

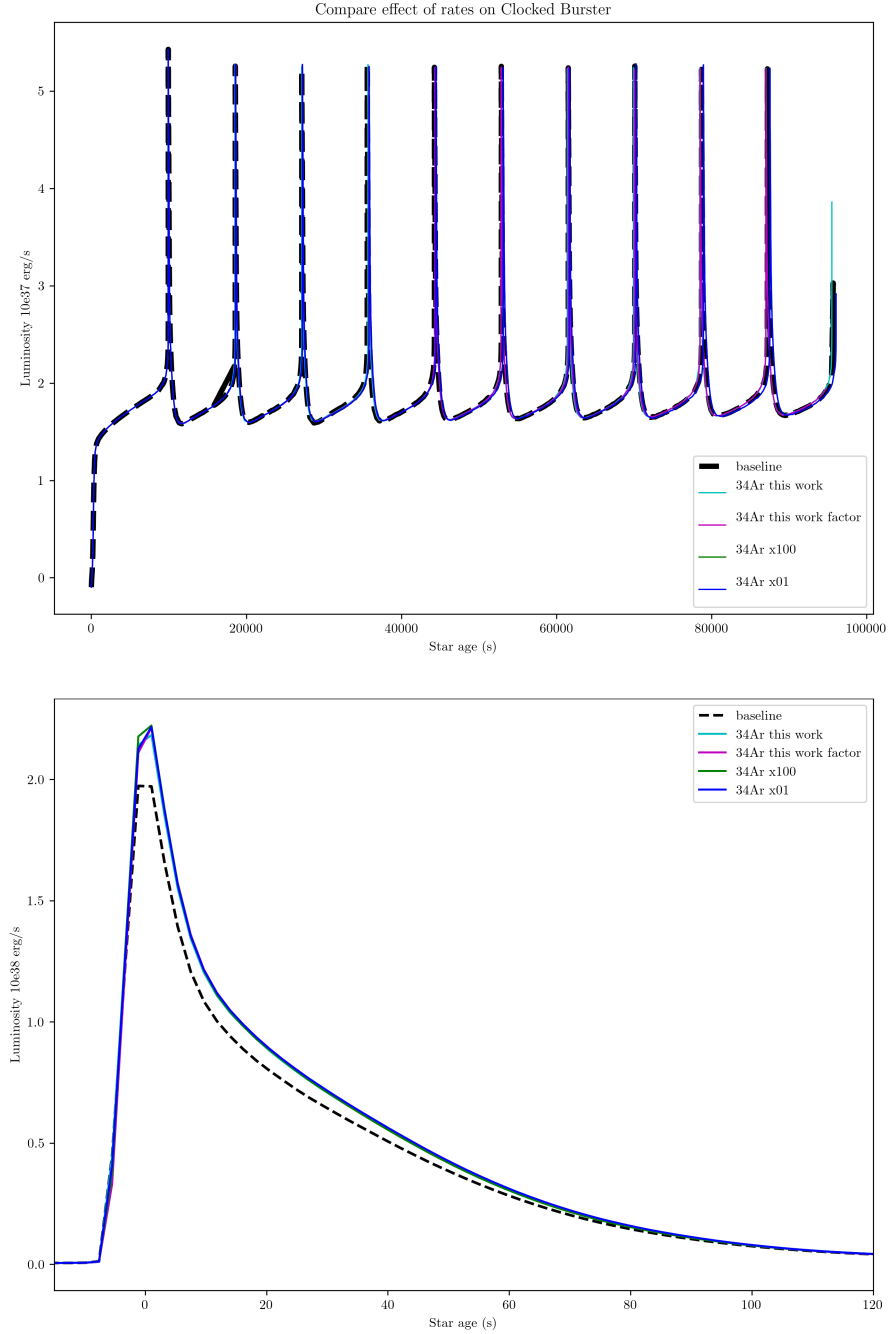


FIG. 4. (TOP) The full series of bursts for the “clocked burster” scenario and accompanying rate variations. (BOTTOM) The luminosity results of each model are averaged and “folded”, such that their peaks are aligned. The resulting plot demonstrates that the variation in burst frequency for the folded light curve caused by changes in reaction rate is not significant enough to be detected on visual inspection. However, variations in the magnitude of the luminosity may explain integrated luminosity variations. Numerical values describing these results are available in Table II.

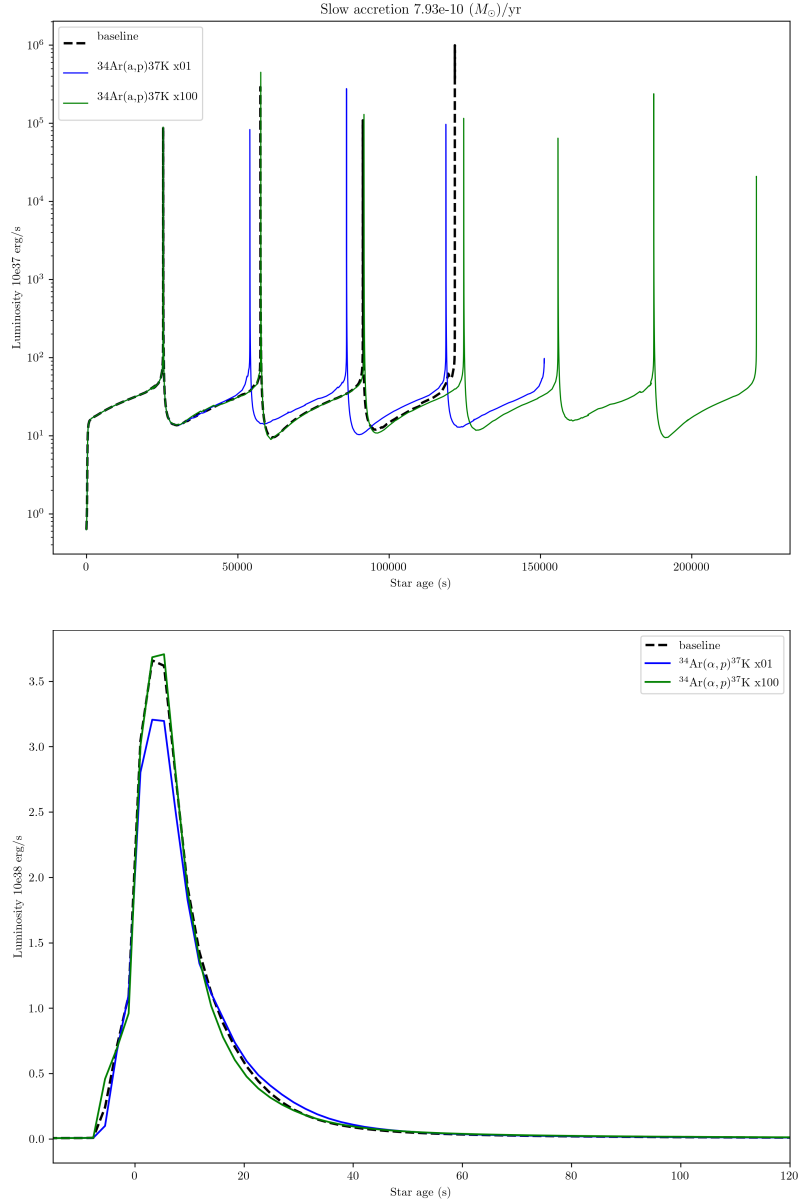


FIG. 5. (TOP) The full series of bursts for the slow accretion scenario and accompanying rate variations. (BOTTOM) The same set of models “folded” such that they are averaged for a given model and their peaks aligned.

caused by variations in the $^{34}\text{Ar}(\alpha, p)^{37}\text{K}$ rate, it is not relevant to this work. The only significant change in burst duration due to this rate variation was in the model using slower accretion (see Fig. 5) with the $^{34}\text{Ar}(\alpha, p)^{37}\text{K}$ rate set at $\times 0.01$ the standard REACLIB rate, which was 2689 s, or 9%, longer. The same model with the rate varied by $\times 100$ showed a slightly smaller variation, while other models varied by $< 1\%$. The absolute maximum luminosity showed more significant variations in the models tested, with the largest variation of 260% again in the slower accretion model with the reaction rate set at 0×0.01 the REACLIB rate, followed by the slow accretion model with reaction rate at $\times 100$ (120%), and the high He-accretion models with the rate at $\times 0.01$ (22%) and $\times 100$ (9%).

The integrated burst luminosity is a metric designed to determine the overall effect on the light curve when a reaction rate is varied, defined in [6] as

TABLE II. Summary of the numerical results of the metrics described in Section V.

Model Identifier	no. bursts	burst period(s)	burst diff%	$M_{LC}^{(i)} 10^{38}$ erg	$L_{max} 10^{38}$ erg/s	L_{max} diff %
Clocked burster						
REACLIB rate	11	8577.07	0.00	0.00	83258.96	0.00
this work	10	8566.84	0.12	6.89	83123.07	-0.16
REACLIB $\times 0.22$	9	8576.47	0.01	7.74	83303.02	0.05
REACLIB $\times 100$	10	8622.79	-0.53	7.38	83657.11	0.48
REACLIB $\times 0.01$	9	8601.35	-0.28	7.82	83113.71	-0.17
high He fraction						
REACLIB rate	4	10649.18	0.00	0.00	474962.17	0.00
REACLIB $\times 0.01$	3	10579.34	0.66	9.95	611728.20	22.36
REACLIB $\times 100$	4	10619.49	0.28	1.13	434371.27	-9.34
slow accretion rate						
REACLIB rate	3	32957.84	0.00	0.00	993079.72	0.00
REACLIB $\times 0.01$	3	30268.30	8.89	5.08	276449.56	-259.23
REACLIB $\times 100$	6	32394.70	1.74	3.22	447802.64	-121.77

$$M_{LC}^{(i)} = \int_{-10}^{150} |\langle L_i(t) \rangle - \langle L_0(t) \rangle| dt, \quad (3)$$

where L_0 is a baseline model with accepted rates from REACLIB [9]. This quantity was similar for all of the ‘‘clocked burster’’ variations. Though these models had similar burst periods and maximum luminosities, variations in burst and quiescent period shape and values could explain these non-zero values (i.e. the differences from the baseline model). The high He-accretion model using the standard reaction rate $\times 0.01$ had the largest $M_{LC}^{(i)}$ value. As this model also had a larger difference in maximum luminosity, this is easier to explain. Both slow accretion models had modest values for this metric.

VI. CONCLUSIONS

Resonances of $^{37}\text{K}+p$ in ^{38}Ca have been studied via proton scattering with a ^{37}K beam on a CH_2 target at the ReA3 facility using a Si detector array and a position-sensitive ionization chamber to determine the excitation function between approximately $E_x = 7.0 - 8.7$ MeV in the ^{38}Ca compound nucleus. In addition to the identification of 13 new levels, the J^π values and proton partial widths of these levels, as well as for levels newly identified by Long *et al.* [11] in this energy range, have been constrained through an R-Matrix analysis of these results. This information was used to estimate a new $^{34}\text{Ar}(\alpha, p)^{37}\text{K}$ reaction rate, which was found to be a factor of 45 less than the standard REACLIB reaction rate, based on Hauser-Feshbach theory. While similar to other indirect studies [11], the rate determined here does not agree with the only previous higher-energy direct measurement [8], which is itself consistent with HF theory.

The sensitivity to this new reaction rate of an XRB model based on GS 1826-24 in MESA astrophysical simulations was studied by comparing the outputs of a baseline model run with the current recommended reaction rate in REACLIB, as well as variations of that rate by factors of 100 up and down, and the rate determined in this work. The results showed no significant deviations in the luminosity profile, burst recurrence time, or burst duration of this initial model when the $^{34}\text{Ar}(\alpha, p)^{37}\text{K}$ rate is varied; however, large variations in the maximum luminosity due to this rate were observed for altered models with slower accretion rates or a larger He fraction. While this does not agree with the results from the single zone models described in Cyburt *et al.* [6] or Browne *et al.* [8], these results are similar to those found in the multizone model of Cyburt *et al.*. It is possible these results could serve as caution against relying heavily on post-processed single-zone models, especially when the nuclear network includes no feedback with the thermodynamics, as is often the case. The results of the variation in abundances may indicate that a 300-species network is not large enough to faithfully explore the XRB scenario. This also suggests that the accepted results, both for this astrophysical scenario and others, derived from a decade or more ago, may need to be revisited considering the vast improvement in computational capabilities over the intervening years. While these results suggest a more precise determination of the $^{34}\text{Ar}(\alpha, p)^{37}\text{K}$ reaction rate is not necessary to better understand XRB nucleosynthesis in GS 1826-24, such a measurement may be useful in determining the applicability of more exotic burst scenarios, as

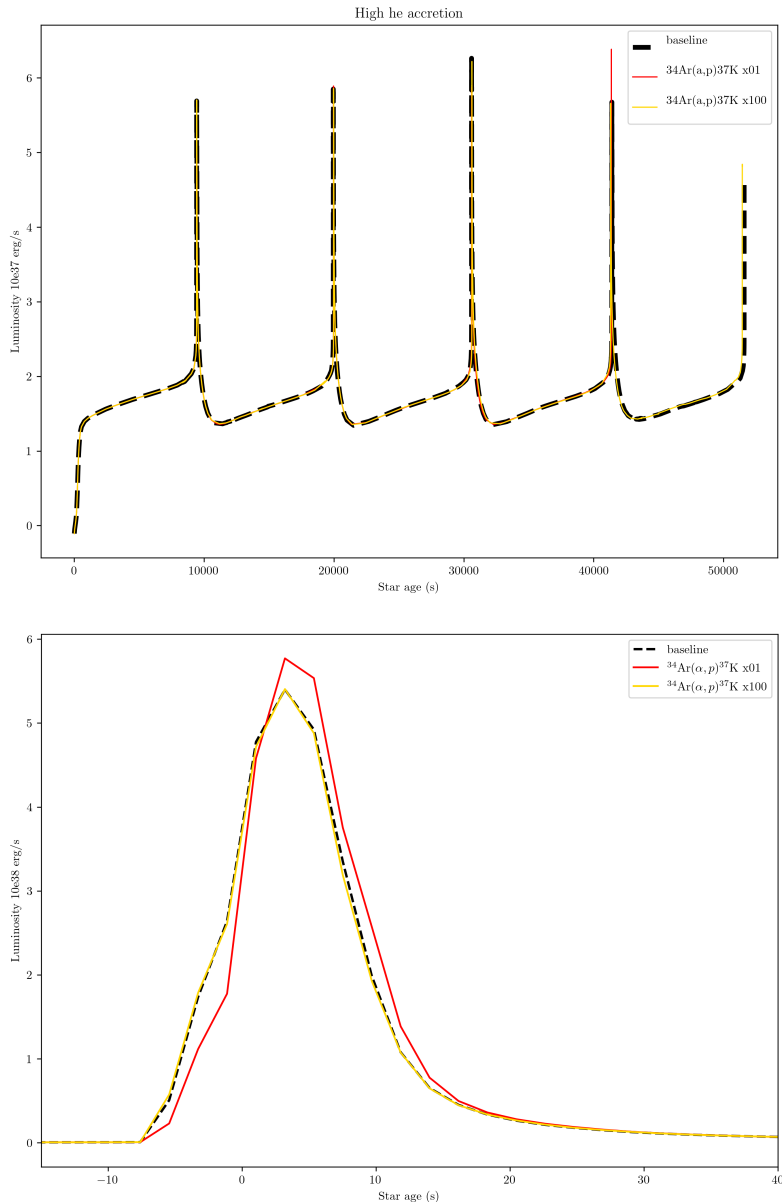


FIG. 6. (TOP) The full series of bursts for the high helium accretion scenario and accompanying rate variations. (BOTTOM) The same set of models “folded” such that they are averaged for a given model and their peaks aligned. Numerical values describing these results are available in Table II.

well as Hauser-Feschbach methods in this mass range given the discrepancies between these results and the accepted HF rate.

VII. ACKNOWLEDGMENTS

This work was partially supported by the U.S. Department of Energy, Office of Science, Office of Nuclear Physics under contract numbers DE-FG02-96ER40978, DOE DE-FG02-02ER41220, DE-AC05-00OR22725, DE-FG02-93ER40773, and DE-AC02-06CH11357, Louisiana Board of Regents RCS Subprogram Contract LEQSF(2012-

15)-RD-A-07, and the National Science Foundation under contract number PHY-1401574.

-
- [1] C. J. Hansen and H. M. van Horn, *The Astrophysical Journal* **195**, 735 (1975).
- [2] H. Schatz and K. E. Rehm, *Nuclear Physics A Special Issue on Nuclear Astrophysics*, **777**, 601 (2006), 0607624.
- [3] W. Pennix, E. Damen, J. Tan, W. H. G. Lewin, and J. van Paradijs, *Astronomy & Astrophysics* **208**, 146 (1989).
- [4] J. L. Fisker, F.-K. K. Thielemann, and M. Wiescher, *The Astrophysical Journal Letters* **608**, L61 (2004).
- [5] S. O'Brien, T. Adachi, G. P. Berg, M. Couder, M. Dozono, H. Fujita, Y. Fujita, J. Görres, K. Hatanaka, D. Ishikawa, T. Kubo, H. Matsubara, Y. Namiki, Y. Ohkuma, H. Okamura, H. J. Ong, N. R. Patel, Y. Sakemi, K. Sault, Y. Shimbara, S. Suzuki, T. Suzuki, A. Tamii, T. Wakasa, R. Wantanabe, M. Wiescher, R. Yamada, J. Zenihiro, and S. O'Brien, *AIP Conference Proceedings* **1090**, 288 (2009).
- [6] R. H. Cyburt, A. M. Amthor, A. Heger, E. Johnson, L. Keek, Z. Meisel, H. Schatz, and K. Smith, *The Astrophysical Journal* **830**, 55 (2016).
- [7] A. Parikh, J. Jose, F. Moreno, C. Iliadis, and J. José, *The Astrophysical Journal, Supplement Series* **178**, 110 (2008).
- [8] J. Browne, K. A. Chipps, K. Schmidt, H. Schatz, S. Ahn, S. D. Pain, F. Montes, W. J. Ong, U. Greife, J. Allen, D. W. Bardayan, J. C. Blackmon, D. Blankstein, S. Cha, K. Y. Chae, M. Febraro, M. R. Hall, K. L. Jones, A. Kontos, Z. Meisel, P. D. O'Malley, K. T. Schmitt, K. Smith, M. S. Smith, P. Thompson, R. Toomey, M. Vostinar, and D. Walter (JENSA Collaboration), *Physics Review Letters* **130**, 212701 (2023).
- [9] R. H. Cyburt, A. M. Amthor, R. Ferguson, Z. Meisel, K. Smith, S. Warren, A. Heger, R. D. Hoffman, T. Rauscher, A. Sakharuk, H. Schatz, F. K. Thielemann, and M. Wiescher, *The Astrophysical Journal, Supplement Series* **189**, 240 (2010).
- [10] T. Rauscher and F.-K. K. Thielemann, *Atomic Data and Nuclear Data Tables* **75**, 1 (2000).
- [11] A. M. Long, T. Adachi, M. Beard, G. P. A. Berg, Z. Buthelezi, J. Carter, M. Couder, R. J. DeBoer, R. W. Fearick, S. V. Förtsch, J. Görres, J. P. Mira, S. H. T. Murray, R. Neveling, P. Papka, F. D. Smit, E. Sideras-Haddad, J. A. Swartz, R. Talwar, I. T. Usman, M. Wiescher, J. J. Van Zyl, and A. Volya, *Physical Review C - Nuclear Physics* **95**, 55803 (2017).
- [12] J. C. Blackmon, K. Macon, C. M. Deibel, B. C. Rasco, D. Santiago-Gonzalez, A. Lauer-Coles, J. Lai, L. Afanasieva, I. Wiedenhöver, L. T. Baby, G. V. Rogachev, E. Koshchiy, H. Schatz, F. Montes, A. Kontos, T. Ahn, and M. L. Avila, *Study of the ^{38}Ca Through $^{37}\text{K}+p$ Scattering to Improve the $^{34}\text{Ar}(\alpha,p)^{37}\text{K}$ reaction rate*, Tech. Rep. (National Superconducting Cyclotron Laboratory, 2014).
- [13] K. Chipps, U. Greife, D. Bardayan, J. Blackmon, A. Kontos, L. Linhardt, M. Matos, S. Pain, S. Pittman, A. Sachs, H. Schatz, K. Schmitt, M. Smith, and P. Thompson, *Nuclear Instruments and Methods in Physics Research Section A: Accelerators, Spectrometers, Detectors and Associated Equipment* **763**, 553 (2014).
- [14] J. Lai, A. Afanasieva, J. C. Blackmon, C. M. Deibel, H. E. Gardiner, A. Lauer, L. E. Linhardt, K. T. Macon, B. C. Rasco, C. Williams, *et al.*, *Nuclear Instruments and Methods of Physics Research Section A* **890**, 119 (2018).
- [15] A. Barnard and C. Kim, *Nuclear Physics* **28**, 428 (1961).
- [16] P. Descouvemont and D. Baye, *Reports on Progress in Physics* **73**, 36301 (2010).
- [17] R. E. Azuma, E. Uberseder, E. C. Simpson, C. R. Brune, H. Costantini, R. J. De Boer, J. Görres, M. Heil, P. J. Leblanc, C. Ugalde, and M. Wiescher, *Physical Review C - Nuclear Physics* **81**, 45805 (2010).
- [18] R. J. de Boer, (2021).
- [19] C. Iliadis, *Nuclear Physics of Stars*, 1st ed. (Wiley-VCH, 2008).
- [20] A. M. Long, *An Indirect Study of the Astrophysical $^{34}\text{Ar}(\alpha,p)^{37}\text{K}$ reaction and its influence on Type-I X-ray Burst Light Curves*, Ph.D. thesis, Notre Dame (2016).
- [21] B. Paxton, P. Marchant, J. Schwab, E. B. Bauer, L. Bildsten, M. Cantiello, L. Dessart, R. Farmer, H. Hu, N. Langer, R. H. D. Townsend, D. M. Townsley, and F. X. Timmes, *The Astrophysical Journal, Supplement Series* **220** (2015), 10.1088/0067-0049/220/1/15, 1506.03146v3.
- [22] D. K. Galloway, A. Cumming, E. Kuulkers, L. Bildsten, D. Chakrabarty, and R. E. Rothschild, *The Astrophysical Journal* **601**, 466 (2004).
- [23] N. Grevesse and A. Sauval, *Space Science Reviews* 1998 85:1 **85**, 161 (1998).
- [24] J. L. Fisker, H. Schatz, and F.-K. Thielemann, *The Astrophysical Journal, Supplement Series* **174**, 261 (2008).